AGU100 ADVANCING EARTH AND SPACE SCIENCE

Earth's Future

RESEARCH ARTICLE
10.1029/2019EF001181

Key Points:
- Water stress estimates can be much different with the consideration of upstream water withdrawal and consumption
- Severe water stress conditions are found in northern China in the past
- Water-stressed areas significantly expand over southern China in the future

Supporting Information:
- Supporting Information S1

Correspondence to:
X. Liu and Q. Tang,
xingcailiu@igsnrr.ac.cn;
tangqh@igsnrr.ac.cn

Citation:
Liu, X., Tang, Q., Liu, W., Veldkamp, T. I. E., Boulange, J., Liu, J., et al. (2019). A spatially explicit assessment of growing water stress in China from the past to the future. *Earth's Future*, *7*, 1027–1043. https://doi.org/10.1029/2019EF001181

Received 10 FEB 2019
Accepted 13 AUG 2019
Accepted article online 19 AUG 2019
Published online 2 SEP 2019

A Spatially Explicit Assessment of Growing Water Stress in China From the Past to the Future

Xingcai Liu[1,2], Qiuhong Tang[1,3], Wenfeng Liu[2,4], Ted I.E. Veldkamp[5,6], Julien Boulange[7], Junguo Liu[8], Yoshihide Wada[6], Zhongwei Huang[1], and Hong Yang[2,9]

[1]Key Laboratory of Water Cycle and Related Land Surface Processes, Institute of Geographic Sciences and Natural Resources Research, Chinese Academy of Sciences, Beijing, China, [2]Eawag, Swiss Federal Institute of Aquatic Science and Technology, Duebendorf, Switzerland, [3]College of Resources and Environment, University of Chinese Academy of Sciences, Beijing, China, [4]Laboratoire des Sciences du Climat et de l'Environnement, LSCE/IPSL, CEA-CNRS-UVSQ, Université Paris-Saclay, Gif-sur-Yvette, France, [5]Institute for Environmental Studies (IVM), Vrije Universiteit Amsterdam, Amsterdam, Netherlands, [6]International Institute for Applied Systems Analysis (IIASA), Laxenburg, Austria, [7]National Institute for Environmental Studies, Tsukuba, Japan, [8]School of Environmental Science and Engineering, Southern University of Science and Technology, Shenzhen, China, [9]Department of Environmental Sciences, MGU, University of Basel, Basel, Switzerland

Abstract In this study, we examine the spatial and temporal characteristics of water stress in China for the historical (1971–2010) and the future (2021–2050) periods using a multimodel simulation approach. Three water stress indices (WSIs), that is, the ratios of water withdrawals to locally generated runoff (WSI_R), to natural streamflow (WSI_Q), and to natural streamflow minus upstream consumptive water withdrawals (WSI_C), are used for the assessment. At the basin level, WSI_R estimates generally match the reported data and indicate severe water stress in most northern basins. At the grid cell level, the WSIs show distinct spatial patterns of water stress wherein WSI_R (WSI_Q) estimates higher (lower) water stress compared to WSI_C. Based on the WSI_C estimates, 368 million people (nearly one third of the total population) are affected by severe water stress annually during the historical period, while WSI_R and WSI_Q suggest 595 and 340 million, respectively. Future projections of WSI_C indicate that more than 600 million people (43% of the total) might be affected by severe water stress, and half of China's land area would be exposed to stress. The found aggravating water stress conditions could be partly attributed to the elevated future water withdrawals. This study emphasizes the necessity of considering explicit upstream and downstream relations with respect to both water availability and water use in water stress assessment and calls for more attention to increasing levels of water stress in China in the coming decades.

Plain Language Summary Severe water stress in China has been widely reported, but its time evolution and spatial patterns are rarely assessed. We examine the spatial and temporal change patterns of water stress in China by using multimodel simulations and three different water stress indices (WSIs). Results suggest that different WSIs imply distinct spatial patterns of water stress over China. The WSIs indicate that water stress conditions in northern China are quite distinct from that in southern China. During the past decades (1971–2010), severe water stress is found in northern areas while little is found in southern areas. In the future (2021–2050), however, water-stressed areas might expand in southern China and water stress levels might aggravate in urban areas, putting considerably more people exposed to severe water stress. This assessment provides useful information for regional water planning/management within the context of future climate change and socioeconomic development in China.

1. Introduction

Water stress refers to economic, social, or environmental problems caused by unmet water needs. Various indicators have been proposed which indicate the level of water demand relative to water availability at a place during a specific period of time (Smakhtin et al., 2004). Many regions of the world have suffered water stress to different extents (Oki & Kanae, 2006; Liu, Yang, et al., 2017). Toward the future, increasing water stress is projected for many regions (including China) of the world due to population growth, socioeconomic development and climate change (Gao et al., 2018; Greve et al., 2018; Schewe et al., 2014; Vörösmarty et al., 2005). Understanding the nature of water stress can assist in developing effective water resources management strategies associated with regional development within the context of global change.

China's total water resources are abundant but unevenly distributed across regions (Liu et al., 2013). The latest survey reported that the annual per capita renewable freshwater availability of China was 2,048 m^3 (http://data.stats.gov.cn), which is about one third of the world's average (~6,184 m^3) according to the World Bank (https://data.worldbank.org). With a growing population and rapid economic development, many areas of China have been experiencing severe water stress for recent decades (Liu, Yang, et al., 2017; Wang et al., 2016). Severe water stress may cause various environmental and social issues, such as reduction of crop production and degraded water quality that threatens human health (Cheng et al., 2009). Water stress in China has been assessed in previous studies at different geographical scales, ranging from provincial level (Cai et al., 2017; Zhao et al., 2015), large river basin level (Gao et al., 2018), to small catchment level (Wang et al., 2016). These assessments demonstrated the general regional feature of water stress and helped understand water stress at relatively large scales in China. However, they often covered short periods (less than 10 years) or only a particular year, thus hampering a thorough documentation of the time evolution of water stress. Moreover, the different time and space scales with which the assessment has been performed allow only up to a limited extent for comparisons between these studies. Water stress in China was also widely reported in global assessments (Alcamo et al., 2000; Hanasaki et al., 2013; Wada et al., 2011; Veldkamp et al., 2015, 2016, 2017) which provided general pictures of water stress in China for both historical and future periods. Nevertheless, the spatiotemporal features and associated drivers (e.g., changes in population, environmental flow, and upstream water resources and withdrawals) were not elaborated due to a global perspective of these studies. Hence, further investigations are required to better understand the spatiotemporal evolution and patterns of water stress in China and its social impacts in terms of the affected population.

To study water stress, several indicators have been proposed (Liu, Yang, et al., 2017), each focusing on different aspects of water stress and having thereby distinct implications. The water stress index (WSI), that is, the ratio of water withdrawals (WW) to water availability (WA), has been developed about two decades ago (Alcamo et al., 2000; Smakhtin et al., 2004; Vörösmarty et al., 2000) and is widely used in various forms in previous assessments (Oki & Kanae, 2006; Veldkamp et al., 2017; Wada et al., 2011). WW is often estimated as the sum of the withdrawals from the agricultural, industrial, and domestic sectors in most previous studies. However, the computation of WA differs. It can be defined as river streamflow (Vörösmarty et al., 2005) or streamflow minus environmental flow (e.g., Hanasaki et al., 2013; Mekonnen et al., 2016). Further, upstream water withdrawals are usually not taken into account in the WSI computation (Wada et al., 2011). Neglecting the upstream-downstream relations with regards to both the streamflow and water withdrawals component may affect WSI estimates to a significant extent. So far, the difference among WSIs, characterized by different methods of calculating WA, is not well understood. How these WSI methods would affect conclusion about the spatiotemporal patterns of water stress assessment is also unclear. It is, therefore, necessary to investigate the influence of applying different WA in the estimation of WSI in order to perform a robust water stress assessment.

To address the abovementioned issues, we perform water stress assessment with various WSIs for the historical (1971–2010) and the future (2021–2050) periods using a multimodel approach. We evaluate how WSI estimates relate to historical observations and try to demonstrate the influence of different methodologies to calculate WA on assessment of water stress. Future water stress conditions are assessed under various scenarios of future WW and WA. The spatiotemporal evolution and patterns of water stress and the population under stress are illustrated with the multimodel simulations at half degree of latitude and longitude grid scale. In doing so, we intend to highlight the necessity of consideration of both upstream water withdrawal and consumption in water stress assessment to deepen our understanding of the water stress situation in China under climate change and socioeconomic developments.

2. Method and Data

Three water stress indices are used to assess water stress in China during the historical (1971–2010) and future (2021–2050) periods. Water resources, water withdrawals, and population data used for water stress assessment are collected from national statistics and multimodel simulations for China covering the two time periods. The method and data set used in this study are described below, and the data and variables for the calculation of water stress indices are summarized in Table S1 in the supporting information.

2.1. Water Stress Indices

WSI, the ratio of WW to WA, is used to quantify water stress assessment in this study. This ratio can represent the ability (and pressure) of meeting the water use requirements based on water resources availability in a specific region. The range of WSI is usually from 0 to 1. A WSI great than 1 means that the water withdrawal exceeds local water availability and is coming from nonrenewable sources or water diversions. The larger a WSI value, the more severe the water stress conditions are. We used the conventional WSI threshold of 0.4 to define the severe water stress (Vörösmarty et al., 2000). Note that a WSI larger than 1 indicates that WW exceeds WA for a specific region. Three WSIs with different WA, namely, $\mathrm{WSI_R}$, $\mathrm{WSI_Q}$, and $\mathrm{WSI_C}$, are calculated on an annual basis. $\mathrm{WSI_R}$ indicates water stress by means of expressing the ratio between WW and the local water resources (i.e., locally generated runoff), $\mathrm{WSI_Q}$ indicates water stress as WW relative to the local and upstream natural streamflow taking account of the environmental flow requirements (EFRs), and $\mathrm{WSI_C}$ indicates water stress as WW relative to the local and upstream natural streamflow taking account of upstream consumptive water withdrawals and EFR.

$$\mathrm{WSI_R} = \frac{\mathrm{WW}_{i,y}}{R_{i,y}}, \tag{1}$$

where $R_{i,y}$ ($\mathrm{m^3}$/year) is total water resources of the ith basin or locally generated runoff of the ith grid cell in the yth year, and $\mathrm{WW}_{i,y}$ ($\mathrm{m^3}$/year) is the water withdrawals of the ith basin or the ith grid cell in the yth year.

$$\mathrm{WSI_Q} = \frac{\mathrm{WW}_{i,y}}{Q_{i,y}}, \tag{2}$$

where $Q_{i,y}$ ($\mathrm{m^3}$/year) and $\mathrm{WW}_{i,y}$ denote the local and upstream natural streamflow taking account of the EFRs and the water withdrawals of the ith grid cell in the yth year, respectively.

$$\mathrm{WSI_C} = \frac{\mathrm{WW}_{i,y}}{\sum_{k=0}^{i} \left(Q_{k,y} - C_{k,y}\right)}, \tag{3}$$

where k numbers the upstream grid cells of the ith grid cell, $Q_{k,y}$ ($\mathrm{m^3}$/year) and $C_{k,y}$ ($\mathrm{m^3}$/year) are local and upstream natural streamflow taking account of EFR and the consumptive water use of the k grid cells in the yth year, respectively. Here $C_{k,y}$ is computed as the product of the consumptive use ratio and the total water withdrawals of the k grid cell in the yth year. $Q_{k,y}$-$C_{k,y}$ can be negative in some grid cells (e.g., in Northwest China) where WW heavily relies on nonrenewable groundwater. In this case, it is set to be zero and $\mathrm{WSI_C}$ is one.

EFR is considered for computing the WSI at the grid cell level (0.5° by 0.5°). EFR is defined as Q90 that the streamflow exceeds 90% of the period of record based on monthly streamflow (Pastor et al., 2014). Subsequently, ERF is subtracted from the monthly streamflow for each grid cell. EFR is not applied to the $\mathrm{WSI_R}$ computation that was performed on the basin level. Water supplies such as interbasin water transfer, rainwater harvesting, and seawater utilization are not considered for the WA estimates in this study. We noted that the conventional threshold of 0.4 for severe water stress takes into account EFR (Hanasaki et al., 2018b); thus, the severe water stress might be overestimated to some extent. However, to find an appropriate threshold that defines severe water stress is out of the scope of this study. Therefore, we used the conventional threshold in the main analysis and perform an additional analysis by using a higher threshold of 0.6 and show the related results in the supporting information.

With the differences between the three WSIs during the historical period, we attempt to illustrate the extent to which water stress assessments could be over/underestimated due to different WA estimation approaches (equations (1)–(3)). Moreover, these differences indicate the cumulative influence of upstream water availability and consumptive water use on downstream water stress. The statistical significance of the difference between $\mathrm{WSI_Q}$ and $\mathrm{WSI_C}$ is examined by applying a Student t test on the annual WSIs time series at individual grid cells.

Based on the WSIs at the grid cell level, the population affected by severe water stress (WSPOP) is estimated to quantify the impacts of water stress on society. Here the population in the grid cells where WSI is greater than 0.4 is counted as WSPOP. In addition, we estimated WSPOP of China using the threshold of 0.6 (see supporting information). Annual WSPOP estimates are averaged over the historical and future periods, respectively, at each grid cell, to examine the spatial patterns of water stress. Finally, we aggregated the annual WSPOP at grid cells for individual basins and China to perform a temporal change analysis.

2.2. Reported Data of Water Withdrawals and Water Resources

Annual water supply from surface water and annual water withdrawals for agricultural, industrial, and domestic sectors in ten major basins of China during the 2001–2010 period were obtained from China Water Resources Bulletin from the Ministry of Water Resources of China (http://www.mwr.gov.cn/sj/tjgb/szygb/). The annual water supply includes interbasin water transfers that usually account for less than 4% of the total water supply of China. However, the quantities of water transferred are not available at the scale of individual basins. The reported data are used to evaluate the skills of the multimodel simulations.

Consumptive use ratio, that is, the ratio between the portion of water that evaporates or is incorporated into a product and no longer available for downstream use and the total water withdrawals, is used for the computation of WSI_C. For each basin, the aggregated consumptive use ratio data for 2001–2003 were obtained from China Water Resources Bulletin (see Table S2), and the mean values over the 3-year data are used for the WSI_C computation at grid cells. Due to data unavailability, we ignore the potential effects on the computation of WSI_C that result from temporal changes in consumptive use ratio over the studied time period.

2.3. Multimodel Simulated Data of Water Withdrawals and Water Resources

2.3.1. Simulations for the Historical Period

Simulated monthly natural streamflow and runoff (surface and subsurface runoff) during the 1971–2010 period are derived from the natural simulations (excluding human impacts) provided by the Inter-Sectoral Impact Model Intercomparison Project phase 2a (ISIMIP2a; Gosling et al., 2017). These simulations were performed by six global hydrological models (GHMs), namely, Distributed Biosphere-Hydrological model (Liu, Tang, Zhang, et al., 2016; Tang et al., 2007, 2008), H08 model (Hanasaki et al., 2008a, 2008b), Lund-Potsdam-Jena managed Land (Biemans et al., 2011; Bondeau et al., 2007; Rost et al., 2008; Schaphoff et al., 2013), Minimal Advanced Treatments of Surface Interaction and Runoff model (Pokhrel et al., 2015; Takata et al., 2003), PCRaster GLOBal Water Balance model (Wada et al., 2014), WaterGAP2 (Flörke et al., 2013; Müller Schmied et al., 2014, 2016) following the ISIMIP2a simulation protocol (https://www.isimip.org/protocol/#isimip2a). These GHMs were forced by three global meteorological forcing products, namely, PGMFD v.2 (Princeton; Sheffield et al., 2006), GSWP3 (http://hydro.iis.u-tokyo.ac.jp/GSWP3/), and a combination of WFD (until 1978; Weedon et al., 2011) and WFDEI (from 1979 onward; Weedon et al., 2014) data sets.

Simulated WW data for the 1971–2010 period are obtained from the globally half-degree data set that is reconstructed by Huang et al. (2018) based on the ISIMIP2a simulations by incorporating reported WW data at the national level. The multimodel simulations of streamflow and WW in China have been evaluated and associated uncertainties have been examined as well in previous studies (Liu, Tang, et al., 2017; Liu, Liu, et al., 2019; Veldkamp et al., 2018).

2.3.2. Projections for the Future Period

For the future period (2021–2050), we used monthly streamflow, total runoff, and WW projected by the H08 (Hanasaki et al., 2008b, 2016, 2018a) and PCRaster GLOBal Water Balance (Wada et al., 2014, 2016) models following the ISIMIP2b protocol (Frieler et al., 2017) to assess the changes in WSIs and WSPOP in China. The two models were driven by four generic circulation models, namely, GFDL-ESM 2M, HadGEM2-ES, IPSL-CM5A-LR, MIROC5 based on the low-emissions representative concentration pathway RCP2.6, and a no-mitigation pathway RCP6.0. In order to utilize as many as possible model ensembles from the ISIMIP2b data set, the projections with fixed socioeconomic conditions (e.g., population, economic development, land use, and management) of the year 2005 (refer to the scenario "2005soc" in Figure 1 in Frieler et al., 2017) were used in this study. The future changes in WSIs and WSPOP are computed by comparing the estimates of the future period to those of the 1971–2000 period for each model ensemble.

For both historical and future periods, multimodel ensembles of annual streamflow and WW are estimated from monthly data at each grid cell, and ensemble medians are computed and then aggregated over

10.1029/2019EF001181

individual basins and China. In this study, we use the multimodel medians for the main analyses, while the 25th and 75th percentiles are calculated to address the spread across GHMs and generic circulation models.

The ISIMIP2a simulations are largely based on meteorological observations or reanalysis and have been widely evaluated in previous studies. In contrast, the ISIMIP2b simulations are based on climate projections, and a bias-correction is performed to make the future WSIs comparable with the historical ones based on ISIMIP2a.

$$\mathrm{WSI}^{*}_{fut,isimip2b} = \left(\mathrm{WSI}_{fut,isimip2b} - \overline{\mathrm{WSI}}_{hist,isimip2b}\right) + \overline{\mathrm{WSI}}_{hist,isimip2a}, \tag{4}$$

where $\mathrm{WSI}_{fut,isimip2b}$ and $\mathrm{WSI}^{*}_{fut,isimip2b}$ are the original and adjusted WSI estimates based on the ISIMIP2b data for the future period 2021–2050, $\overline{\mathrm{WSI}}_{hist,isimip2b}$ and $\overline{\mathrm{WSI}}_{hist,isimip2a}$ are multimodel medians of multiyear mean WSI over the 1971–2000 period based on the ISIMIP2a and ISIMIP2b data, respectively. $\mathrm{WSI}^{*}_{fut,isimip2b}$ is used for future water stress assessment.

2.4. Population

The spatially distributed (1 km × 1 km) population data of China in 1995, 2000, 2003, 2005, and 2010 were obtained from National Earth System Science Data Sharing Infrastructure, National Science and Technology Infrastructure of China (http://www.geodata.cn). We upscaled the reported population data from 1 km to half degree by summating the data of 1-km grid cells in a half-degree grid cell. The population in the years between 1995 and 2010 was estimated by means of a linear interpolation using the available data. The population prior to 1995 was estimated by disaggregating the annual population of China (from http://data.stats.gov.cn/) according to the spatial patterns of the year 1995.

As for the future projections, the population of China during the 2021–2050 period was derived from a global population data set with a spatial resolution of half-degree based on SSP1 and SSP2 scenarios (Jones & O'Neill, 2016). The SSP1 (the sustainability scenario) and SSP2 population estimates are used to calculate water-stressed population under RCP2.6 and RCP6.0, respectively. We note that the spatial coverages of the historical population (Figure S1a) and the future population (Figures S1c and S1d) are slightly different, mostly in Northwest China. Nevertheless, the data was not further modified since the differences are small (Figures S1e and S1f) and is not anticipated to have significant influences on the overall assessment.

The areas with high population density (larger than 3 million people in a grid cell in the year 2021) in the future are identified as where large cities may exist. The WSPOP in these areas is estimated to examine the contribution of the increasing population in urban areas on future water stress.

3. Results

3.1. Evaluation of the Multimodel Simulations of Water Stress

The multiyear mean $\mathrm{WSI_R}$ based on the reported data by China Water Resources Bulletin is compared with the ISIMIP2a simulations over the 2001–2010 period for 10 river basins (Figure 1). The reported data show that severe water stress ($\mathrm{WSI_R} > 0.4$) occurred in most northern basins except for the Songhua River, while no water stress was found for the southern basins during this period. The Hai River has the largest water stress with a $\mathrm{WSI_R}$ of 1.56, followed by the Huai River ($\mathrm{WSI_R} = 0.64$) and the Yellow River ($\mathrm{WSI_R} = 0.62$). The reported $\mathrm{WSI_R}$ is less than 0.2 in all southern basins. However, moderate water stress conditions might exist in the Yangtze River and the Pearl River, which have a $\mathrm{WSI_R}$ of 0.19, during this decade. Generally, moderate water stress ($\mathrm{WSI_R} = 0.21$) is found for China as a whole. The simulated $\mathrm{WSI_R}$ indicates water stress conditions that are similar to the reported data. On average, the simulated $\mathrm{WSI_R}$ of China is 5% lower than the reported one. The deviations are mainly due to the overestimation of WW in the northern basins and the underestimation of WW in the southern basins (see Table S3). Overall, the simulated water stress is generally consistent with those based on the reported data.

The contributions of different sectoral WW on the $\mathrm{WSI_R}$ are indicated by the different color of the bars in Figure 1 for both the simulated and reported data. The agricultural WW is found to be dominant in all basins, causing severe water stress in the Northwest Rivers, the Hai River, the Yellow River, and the Huai River. The second major WW sector is identified as the industrial WW for all basins. The reported data show that the agricultural WW contributes about 50% to 94% to the $\mathrm{WSI_R}$ over basins and contributes 65% of the

10.1029/2019EF001181

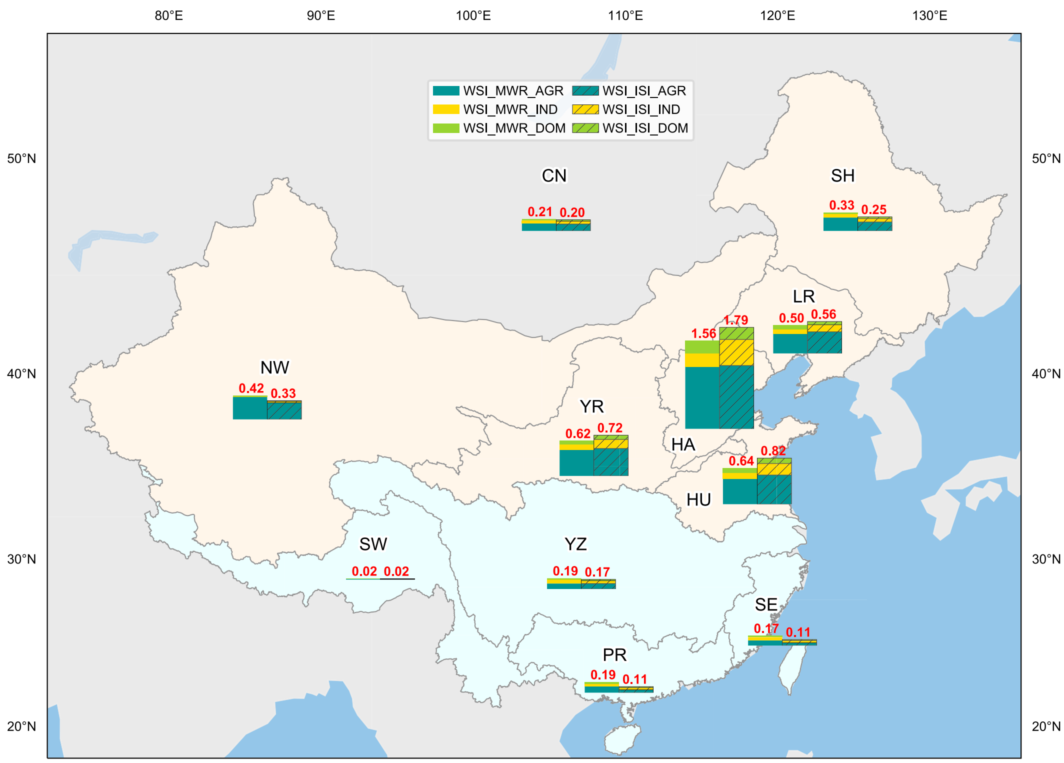

Figure 1. Mean water stress index based on runoff (WSI_R) in the major basins and China over the 2001–2010 period. MWR (not hatched) indicates the WSI_R estimates based on Ministry of Water Resources (MWR) reported water withdrawals and total water resources data, while ISI (hatched) indicates the estimates based on the Inter-sectoral Impact Model Intercomparison Project 2a (ISIMIP2a) simulations. AGR indicates the agricultural sector, DOM indicates the domestic sector, and IND indicates the industrial sector. Southern basins: Yangtze River (YZ), Southeast Rivers (SE), Southwest Rivers (SW), Pearl River (PR). Northern basins: Songhua River (SH), Liao River (LR), Northwest Rivers (NW), Yellow River (YR), Hai River (HA), and Huai River (HU). CN denotes the whole of China.

WSI_R of China, on average (see the numbers in Table S4). Industrial WW contributes 15% to 36% to the WSI_R in most basins (except in the Northwest Rivers and the Southwest Rivers where the industry is less developed). Overall in China, industrial WW contributes more than 20% of the WSI_R on average. The contribution of domestic WW is the largest in the Pearl River (17%) and the smallest in the Northwest Rivers (3%). The simulations based on ISIMIP2a indicate similar contributions of the sectoral WW to WSI_R. The simulations indicate a higher contribution of industrial WW than reported data except in the Huai River and higher contributions of the domestic WW in most basins (see the relative errors in Table S4).

3.2. Spatiotemporal Changes in Water Stress Based on WSI_R in the Past

The simulated annual WSI_R vary significantly between the northern and southern basins over the 1971–2010 period (Figure 2). The distinct patterns of water stress in Figures 2a and 2b are mainly due to the relatively large WW and low WA in the northern basins and the opposite situations in the southern basins (see Table S3). Severe water stress is found for all years in the Hai River, the Huai River, the Yellow River, and the Liao River. The largest WSI_R is found in the Hai River where it is greater than 1 in 70% of years. Next are the WSI_R in the Huai River and Yellow River, where values greater than 0.4 are found for all years while mean values are 0.84 and 0.68 over the historical period, respectively. Severe water stress is found in the Liao River for many years, while the severity is less in the Northwest Rivers. Moderate water stress is found in the Songhua River where the annual WSI_R is around 0.2. Water stress in the southern basins, with annual WSI_R below 0.2, is much smaller than that in the northern basins. The WSI_R of Southwest Rivers is the smallest, which is estimated at around 0.01 during the historical period. WSI_R of China is less than 0.2 for most years except the last several years.

The linear trends in the annual WA, WW, and WSI_R during the 1971–2010 period are shown in Table S5. No significant trends are found for WA (tested by a *t* test at the 95% confidence level, the same hereafter), while

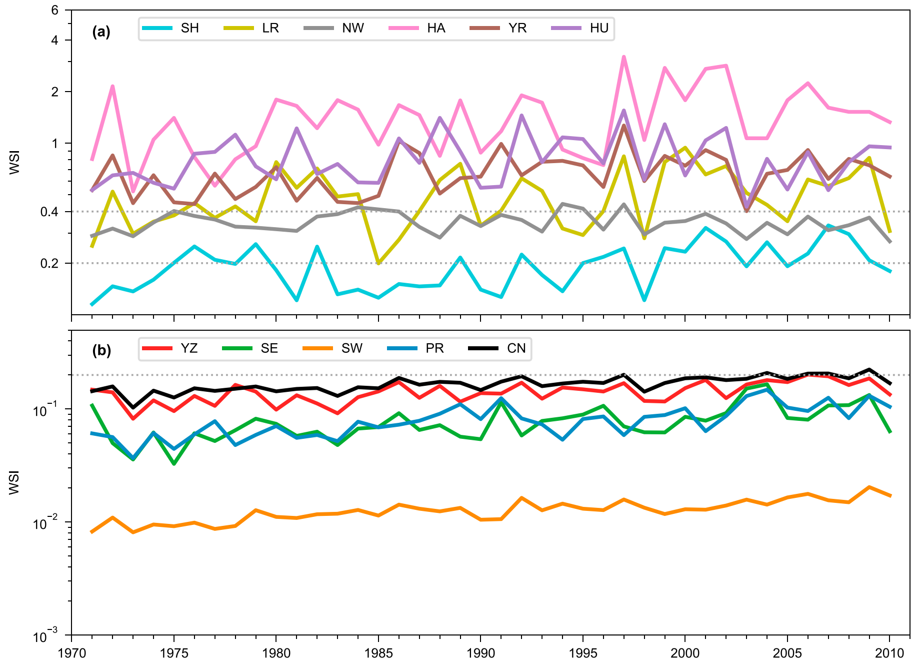

Figure 2. Annual water stress index in the northern basins (a) and southern basins and China (b) during 1971–2010. A log scale is used for the *Y* axis in (a) for a better view. The acronyms in the legends indicate the basin names in Figure 1.

statistically significant upward trends in WW are found for all basins except the Northwest Rivers. Consequently, the WSI_R shows statistically significant upward trends in most basins except the Northwest Rivers and the Yangtze River. The upward trends in WSI_R could be largely due to the significant increase of WW. Statistically significant increases in WW and WSI_R are found for China as a whole.

3.3. Comparison of Water Stress and Affected Population Based on WSIs

The spatial distribution of the mean annual WSI over the 1971–2010 period indicated by the three WSIs are illustrated in Figure 3. Generally, the spatial patterns of WSI are similar to that of the cropland (see Figure S1b) further underlining the dominant role of the agricultural sector in water stress. WSI_R (Figure 3a) shows heightened water stress compared to WSI_Q (Figure 3b) and WSI_C (Figure 3c), not only in terms of severity but also in terms of spatial distribution. Widespread large values of WSI_R (mostly greater than 1, i.e., all local runoff is used) indicate extreme water stress in many areas of the northern basins. Severe water stress, indicated by WSI_R (WSI > 0.4), is also found in upper reaches and a few grid cells in the lower reaches of the Yangtze River. Severe water stress indicated by WSI_Q is mainly found in the northern basins and in addition to a few grid cells in the Yangtze River (Figure 3b). The water stress indicated by WSI_C (Figure 3c) shows very similar spatial patterns as WSI_Q but is a little more severe. The differences between WSI_C and WSI_Q (Figure 3d) are relatively large and statistically significant in some northern areas (indicated by blue dots). It suggests that the differences can be more significant in the areas with higher water stress. There are often abundant local water resources in the southern basins, thus the consumptive water withdrawals may not reduce much water availability. These results indicate that the water withdrawals significantly exceed the locally generated water resources in many northern regions, and water stress would be underestimated without the consideration of the consumptive water use.

The spatial distributions of WSPOP for the historical period (Figure 4) are similar to the spatial patterns of WSIs (see Figure 3). An exception is that the population affected by severe water stress is relatively small in the Northwest Rivers because of the low population density there. A large population is affected by severe water stress in the Hai River and Huai River where population density is high. As indicated by WSI_R (Figure 4a), severe water stress can be found in almost all areas of the Hai River and Huai River and most areas of the Yellow River and the Liao River. During the 1971–2010 period, 42% (39% and 55% for the 25th and 75th percentiles), 40% (26% and 45%), and 39% (25% and 43%) of the total area of China experienced

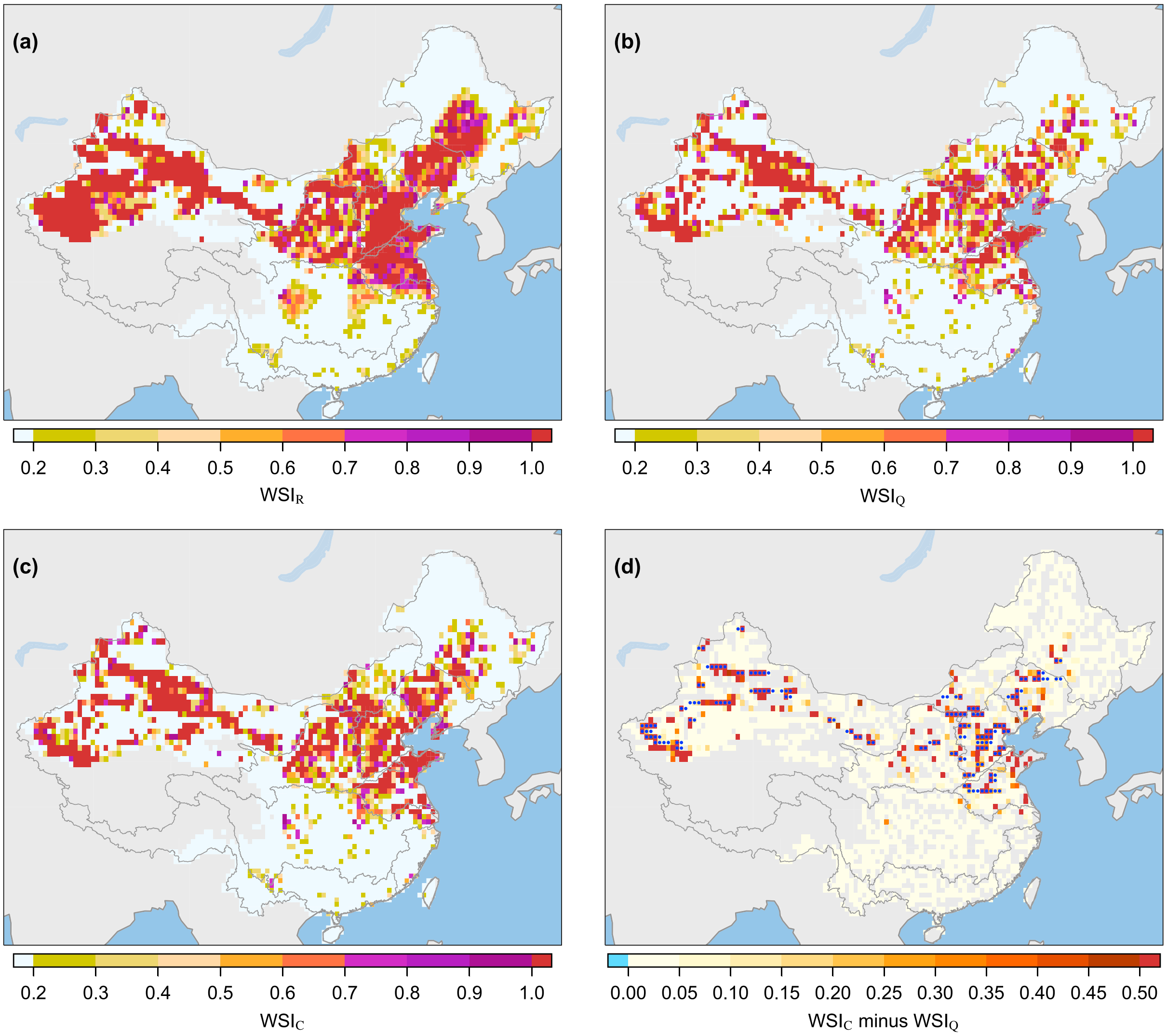

Figure 3. Mean annual water stress in China over the 1971–2010 period indicated by the (a) water stress index based on runoff (WSI_R), (b) water stress index based on streamflow (WSI_Q), (c) the water stress index based on streamflow subtracting consumption (WSI_C), and the (d) difference between WSI_C and WSI_Q. The blue dots in (d) indicate that the difference between WSI_C and WSI_Q is statistically significant based on a student *t* test at the 95% confidence level.

severe water stress every year indicated by WSI_R, WSI_C, and WSI_Q, respectively, while 54% (50% and 59% for the 25th and 75th percentiles), 33% (26% and 36%), and 30% (24% and 33%) of the total population were affected, respectively. The difference in WSPOP between WSI_C and WSI_Q is small in most areas since large differences between the two WSIs mostly appear in the areas with high WSI_Q (greater than 0.4) and hence do not have a visible influence on the population and/or land area being affected by severe water stress or not.

The annual WSPOP and the corresponding fractions relative to the total population show a statistically significant increase during the historical period (see the inner plots in Figure 4). The WSPOP based on WSI_R is the largest (458 to 750 million), accounting for ~50% in the 1970s to ~60% in the 2000s of the total population of China. In contrast, WSI_C indicates 260 to 470 million of WSPOP, accounting for ~29% (1970s) to ~37% (2000s), being slightly larger than that based on WSI_Q (26% to 34%). The multiyear mean WSPOP based on the WSI_R (WSI_Q) is 595 (340) million, which is 62% higher (8% lower) than the 368 million based on the WSI_C. The differences between the annual WSPOP and the corresponding fractions (the inner plot in Figure 4d) based on WSI_Q and WSI_C show a statistically significant increasing trend. The WSPOP metrics further show that the impacts of severe water stress are much larger in the northern basins than in the southern basins.

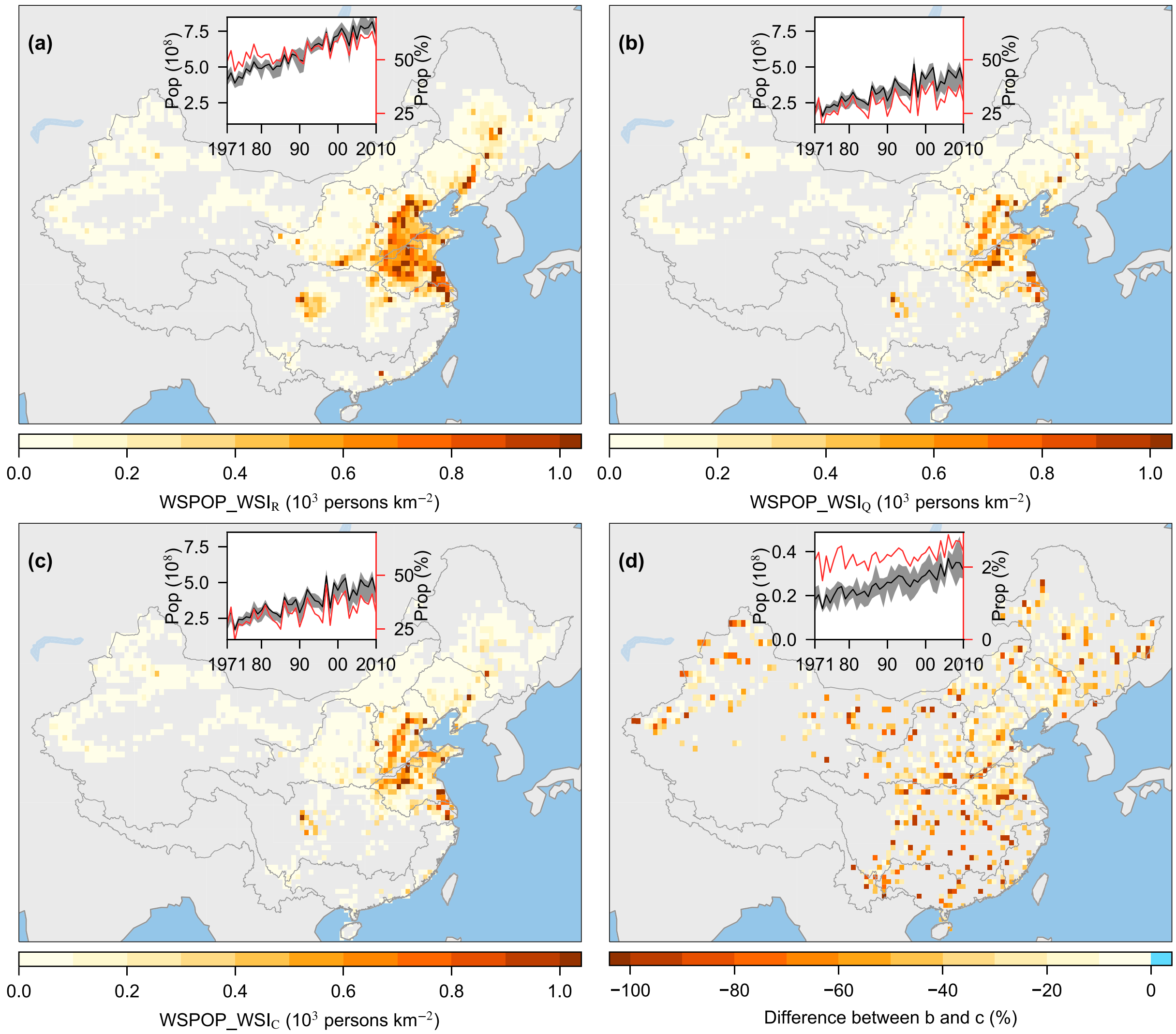

Figure 4. Multimodel medians of the mean annual population affected by water stress in China using water stress index based on runoff (WSI$_R$; a), water stress index based on natural streamflow (WSI$_Q$; b), and water stress index with consideration of consumption (WSI$_C$; c) over the 1971–2010 period. The difference between (b) and (c) is shown in panel (d). The annual population affected by severe water stress (WSPOP; black line) and their proportions (blue line) relative to the annual total population are shown in the inner plots. The shaded areas show the 25th and 75th percentiles of annual WSPOP.

3.4. Projected Water Stress in the Future

Considering significant differences among the three WSIs, the analysis of water stress is mainly based on WSI$_C$ for the future time period, with the results of WSI$_R$ and WSI$_Q$ shown in the supporting information. WSI$_C$ plausibly provides more reasonable estimates of water stress of the real world by considering both upstream water availability and upstream consumptive water withdrawals, thus is regarded as more appropriate for future water stress assessment. The simulated multiyear mean annual WSI$_C$ over the future period (2021–2050) show similar spatial patterns for RCP2.6 and RCP6.0 (Figure 5), that is, WSI$_C$ is large in the northern basins and relatively small in the southern basins. For RCP2.6, the multiyear mean annual WSI$_C$ is greater than 0.4 (1.0) in 31% (18%) of the total areas of China. The percentages are 32% and 18% for RCP6.0. The future annual WSI$_C$ for the whole of China (see inner plots in Figures 5a and 5b) would be less than 0.2 for most years. The projections of WSI$_R$ and WSI$_Q$ also show intensified water stress (see Figure S3). WSI$_R$ indicates higher while WSI$_Q$ indicates slightly lower water stress in comparison with WSI$_C$, which are similar to the differences during the historical period (see Figure 3).

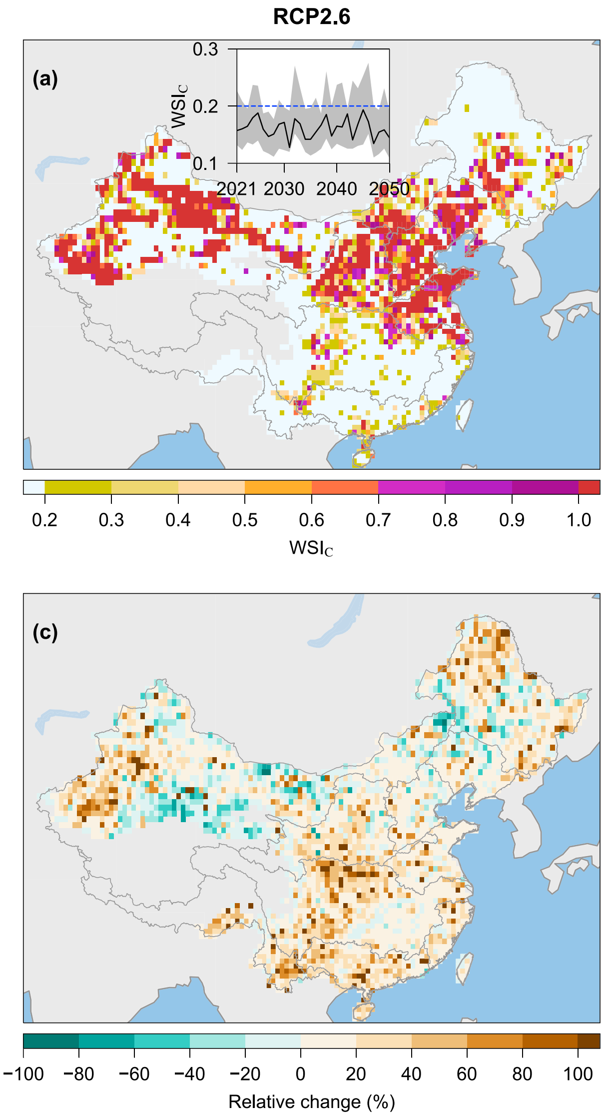

Figure 5. Multimodel medians of mean annual water stress (WSI$_C$) in China over the 2021–2050 period under RCP2.6 (a) and RCP6.0 (b), and the corresponding relative changes (c and d) compared with those in the historical period. The annual WSI$_C$ for the whole of China is shown in the inner plots, where the shaded areas denote the 25th and 75th percentiles.

Compared to the historical period, the southern basins would experience increases in WSI$_C$ toward the future, while many northern areas face decreases in WSI$_C$ for both RCP2.6 (Figure 5c) and RCP6.0 (Figure 5d). WSI$_C$ would increase in more than 70% of total areas and will increase by more than 50% in about 12% of the total areas of China for both RCPs. Relative changes of more than 100% are mostly found in the middle reaches of the Yangtze River and some parts of the Pearl River, Northwest Rivers, and the Songhua River. WSI$_C$ would decrease in large parts of the Northwest Rivers and some parts of the Liao River and the Songhua River. Small changes are found in the Huai River and the Hai River. Changes in future streamflow (see Figure S2) show strong similarities to the changes in future WSI$_C$. For both streamflow and WSI$_C$, we find increases in the northern basins but decreases in the southern basins.

For the future period, the spatial distribution of WSPOP is very close for the two RCPs (Figures 6a and 6b). The WSPOP is larger in the northern basins than that in the southern basins. High annual WSPOP, as many as 1,000 persons/km^2, mainly appear in the Hai River, the Huai River, and some coastal areas. This is due to both the high WSI$_C$ (Figure 5) and the high population density (see Figure S1) in these regions in the future.

10.1029/2019EF001181

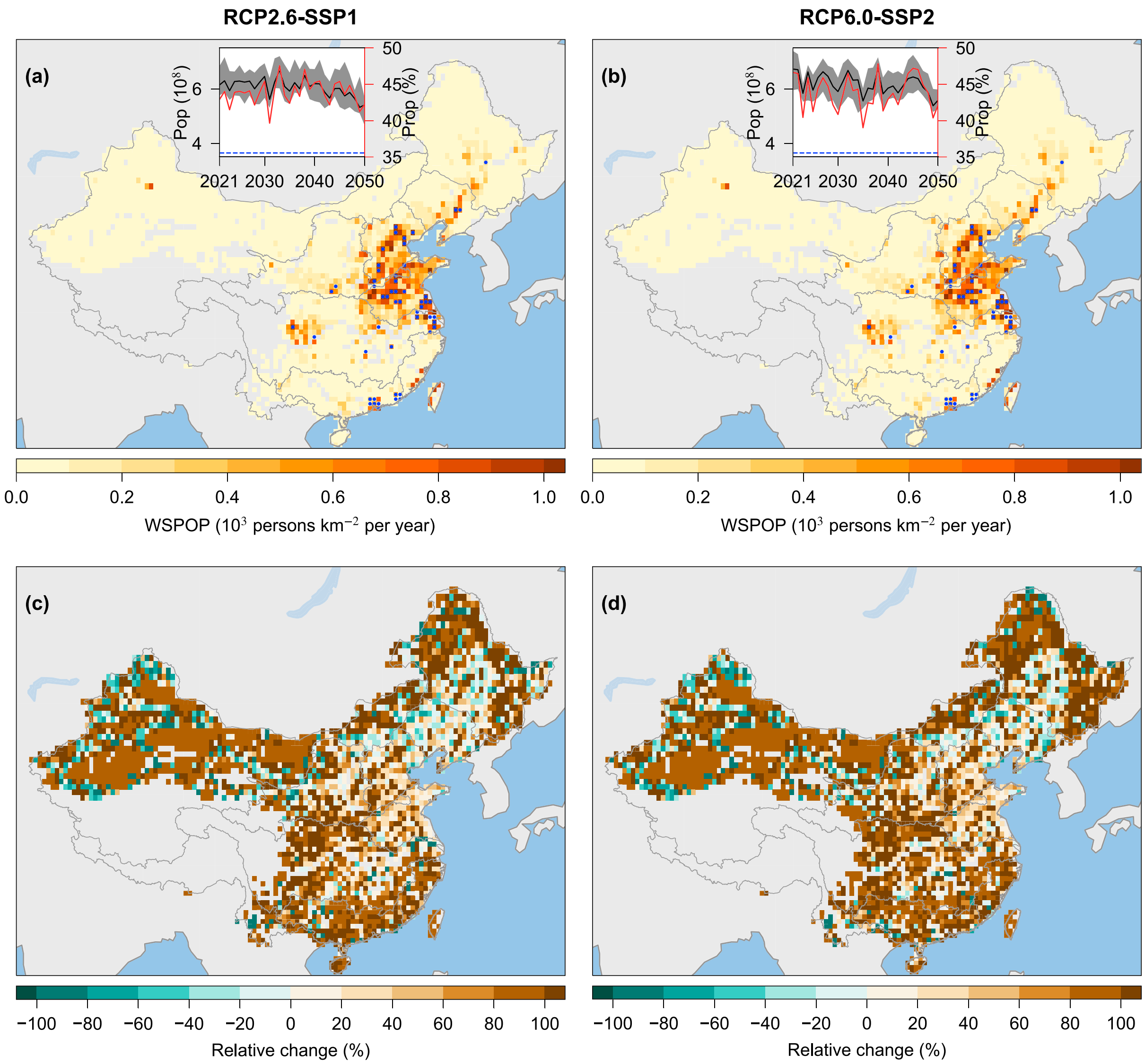

Figure 6. Multimodel medians of the mean annual water-stressed population indicated by WSI_C in China over the 2021–2050 period for RCP2.6-SSP1 scenario (a) and RCP6.0-SSP2 scenario (b), and their relative changes (c and d) compared with the historical period.

The areas affected by severe water stress will significantly expand, especially in the southern basins where water stress only occurred in a few areas in the past. More than 80% of the total areas of China might experience severe water stress in at least 1 year during the future period for both RCPs. Severe water stress might appear in about 48% (40% and 55% for the 25th and 75th percentiles) and 49% (40% and 56% the 25th and 75th percentiles) of the total areas of China every year under RCP2.6 and RCP6.0, respectively. The multiyear mean WSPOP for the whole of China might be 612 million (542 and 668 for the 25th and 75th percentiles) and 618 (560 and 680 for the 25th and 75th percentiles) for RCP2.6 and RCP6.0, respectively. These WSPOPs account for about 43% of the total population in the future (see relative numbers in Table S6).

The multiyear mean WSPOP might increase in most parts (about 70%) of China, while decreases are found in the Northwest Rivers, the Liao River, and the Songhua River (Figures 6c and 6d). These spatial patterns are similar to those of the WSI_C (see Figures 5c and 5d). The relative changes are large (greater than 100%) in considerable areas of the southern basins, such as the upper reaches of the Yangtze River and many coastal areas. The WSPOP changes are in line with the population change at many grid cells; in particular, the decrease in WSPOP mostly appears in the areas with population decrease (see Figure S4).

Fifty-two grid cells are identified as urban areas (with larger than 3 million people in the year 2021) in China (see the blue dots in Figures 6a and 6b) for both RCP2.6 and RCP6.0. In these areas, more than 110 (100 and 117 for the 25th and 75th percentiles across RCPs) million people would be affected by severe water stress during the 2021–2050 period, on average, accounting for nearly 20% of the total WSPOP for both RCPs (Figure 7). Compared to the historical period, the WSPOP in the urban areas would increase by about 70% for both RCPs during 2021–2050, which is greatly larger than the average of China (49%). The mean WSPOP estimates under RCP2.6 and RCP6.0 are very close to each other over the 2021–2050 period, but the interannual variations of the WSPOP are different for these two scenarios. There are little temporal variations of population change (Figure S1). The large and distinct interannual variations of the WSPOP are largely associated with interannual variation of streamflow (Figure S2).

4. Discussion

In this study, we evaluate and analyzed various WSI that include and exclude upstream water availability, water withdrawals, and environmental flow requirements using multimodel simulations over historical and future time periods. An evaluation with reported data over the period 2001–2010 shows that simulations and observations generally match well in the major basins of China. Our historical water stress assessment over the 1971–2010 period suggests that water stress was severe in the northern basins and was mild in the southern basins but significantly increased over the historical time period. Future water stress assessment based on WSI_C indicates that more severe water stress will emerge in both northern and southern China under climate change and socioeconomic development and the increasing number of water-stressed population can be partly attributed to the population growth which not only increase water withdrawals and also increase the exposure to water stress.

4.1. Significant Differences Between WSIs

Over the historical period, the three WSIs show generally similar spatial patterns of water stress, that is, higher WSI in north and lower in south, but distinct levels of water stress. At the grid cell level, the WA for the three WSIs, that is, locally generated runoff, local and upstream natural streamflow taking account of EFR, and local and upstream natural streamflow taking account of upstream consumptive water withdrawals and EFR, differs significantly in many regions. The WA differences result in evidently higher water stress based on WSI_R and lower water stress based on WSI_Q. The spatial patterns of WSI_R, with widespread higher levels of water stress in northern areas, are particularly different from the other two. This underlines the importance of upstream water resources in meeting downstream water demand in these regions. The southern basins have a relatively wetter climate and most water uses could be met by local runoff; thus, severe water stress is rarely indicated by all three WSIs during the historical period (Figure 3). The different levels of water stress between the northern and southern basins have also been reported over different historical periods (Cai et al., 2017; Liu, Yang, et al., 2017; Wang et al., 2016). The WA differences among these WSIs could be even larger when considering interbasin water transfer, reservoir regulation, etc., or performing a seasonal assessment. In regarding water transfer, the WSI might be overestimated in the basins accepting water while it might be underestimated in the basins that export water resources.

The differences in water stress indicated by the WSIs are also clearly displayed in terms of population. The WSPOP of China indicated by WSI_R is 60% higher compared to WSI_C in the historical period, while the WSPOP based on WSI_Q can be 8% lower without excluding the consumptive water use that is not reusable on the river network. Thus, in other words, reuse as an alternative to the reduction of water withdrawals could also alleviate downstream water stress. Though subject to uncertainties as we discuss below, WSI_C plausibly provides more reasonable estimates of water stress conditions of the real world among the three WSIs and therefore is recommended for future water stress assessment.

4.2. Distinct Spatial Patterns of Water Stress From Northern to Southern China

All three WSIs show distinct spatial patterns of water stress from north to south of China. In the past decades, very little water stress is found in the southern basins while severe water stress is particularly prominent in the northern basins of China. The high WSIs indicate that renewable freshwater resources can hardly meet water demand and, consequently, lead to significant environmental and social issues in northern China (Cai, 2008). More than half of China's population inhabits in the northern basins, among which

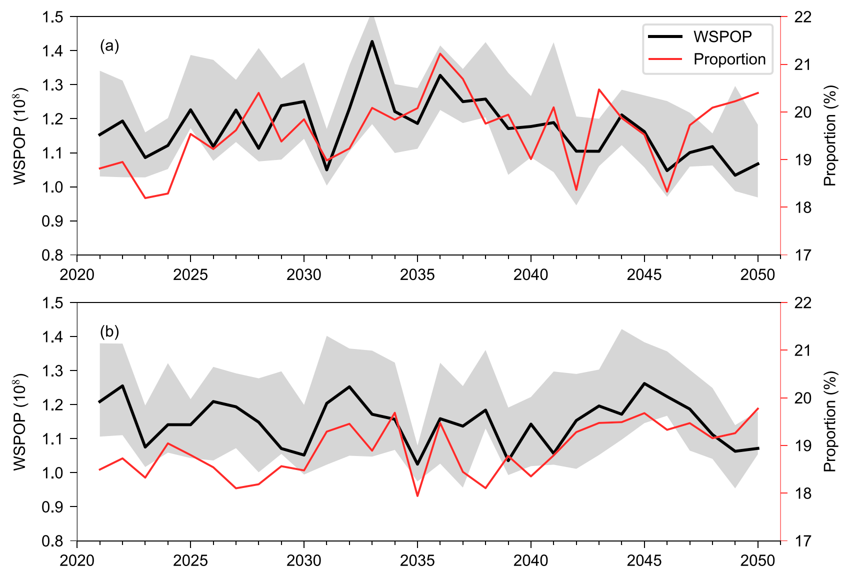

Figure 7. The water-stressed population (WSPOP) in urban areas for the RCP2.6-SSP1 (a) and RCP6.0-SSP2 (b) scenarios. The black lines denote the multimodel median of WSPOP in urban areas and the grey areas denote the range of 25the and 75th percentiles across multimodel ensembles. The red lines denote the proportion of the WSPOP in urban areas to the total WSPOP of China. The urban areas are identified the grid cells with a population greater than 3 million.

the Hai River and Huai River own the second and the third largest population. The WSPOP in these two basins accounts for more than 40% of the total WSPOP indicated by WSI_C. The severe water stress but relatively low WSPOP in the Northwest Rivers indicate that this basin is a water-exporting region, which might have aggravated the water stress (Zhao et al., 2015). In order to alleviate water stress, a large amount of groundwater has been pumped for human water use (Liu et al., 2001; Tang et al., 2013), and on the other hand, various measurements, such as controlling the total water withdrawals, improving water use efficiency, water diversion, and optimization of water allocation, have been proposed during the past decades (Cheng et al., 2009; Wang et al., 2017; Yang & Zehnder, 2001). However, most of these measures were not explicitly represented in the multimodel simulations, thereby further investigation is needed to evaluate the effects of the measures on water stress.

In the future, water stress might be more severe in northern basins and considerably expand in the southern basins where it used to occur only seldom as indicated by the low WSIs conditions. The population clustering in the Hai River and Huai River might aggravate the water stress there. In southern China, severe water stress would mostly appear in the areas with high population density (see the future population in Figure S1), such as the coastal regions and the lower reaches of the Yangtze River. A large population lives in these developed eastern regions which take the lead in China's economy. The increasing water stress levels in these regions can have significant socioeconomic implications, for example, an increasing constraint on the development of a high-quality economy.

4.3. Major Contributors to the Changes in WSIs

The projected changes in WSIs are largely related to the changes in WW and WA. In the future, WW is projected to increase significantly (by more than 50%) across China (Figures S2a and S2b), while the projections of runoff and discharge generally show a spatial pattern of increase in north and decrease in south (Figures S2c–S2f; see also Liu, Tang, Voisin, et al., 2016, which used the ISIMIP fast-track data set). The increase in WW undoubtedly result in more severe water stress while the increase in WA would, to some degree, alleviate water stress conditions in northern China (mostly in the Northwest Rivers; see also Figures 5c and 5d). In southern China, though the relative smaller change in WW, the decreases in total water resources resulting from climate change might lead to considerable expansion of area suffering severe water stress. Note that population growth is greatly associated with the changes in WW; meanwhile, it increases the exposure of the population to severe water stress.

For mitigating water stress in these regions, both climate change and socioeconomic development should be considered (Liu, Antonelli, et al., 2019). For example, an adaptive scheme of reservoir regulations and reallocation of water resources would partly offset the impact of hydrological changes. Promoting water use efficiency via technological improvement is also an important way for the mitigation of future water stress. Nevertheless, facing the higher water stress in the future, how the integrated solutions can be implemented would remain a great challenge in these regions (Cheng & Hu, 2011; Greve et al., 2018).

4.4. Effect of the Population Estimates on Water Stress Assessment

Future water stress in terms of WSPOP is evidently related to the population change (see Figure S4). The decrease in population in some regions (see Figure S1) might reduce the WSPOP in the future. However, the prevalent increase of WW would result in expanded severe water stress across China and eventually more people will be affected (Figures 6a and 6b). The effect of future population change to the WSPOP estimates is examined by calculating WSPOP with the fixed population (and its distribution) of China of the year of 2010. This WSPOP (see Figure S5) shows very similar spatial patterns as Figure 6, and the total WSPOP would be about 584 and 581 million for RCP2.6 and RCP6.0, respectively, which are 6% and 7% lower, respectively, compared to the WSPOP estimates with population growth. The relative changes in Figure S5 are slightly smaller than those in Figure 6. We note that China's population will clearly decrease after around 2030, while no similar trends are found in the annual WSPOP (see the inner plots in Figure 6). This indicates that the WSPOP (and WSI_C) would be even larger if the population remains at the level of 2030. Population change may influence WSI estimates by altering (domestic) water use requirements (e.g., in the southern basins), which also indirectly affect the WSPOP estimates. Multimodel studies considering transient socioeconomic conditions (e.g., changes in population, economic development, land use, and management) are needed to improve the projections of future water stress conditions.

WSPOP may be overestimated because the population exposed to severe water stress is not necessarily affected on a half-degree spatial scale. Particularly, the impacts of severe water stress on urban and rural population are different, for example, water stress result from agricultural irrigation may not affect the urban population. Further investigation with high-resolution hydrological data set and urban population data could benefit the evaluation of water stress arising from the expansion of urban areas and increasing urban population in China.

4.5. Uncertainty in the Water Stress Assessment

Uncertainty sources in water scarcity assessment have been well documented by a recent study (Greve et al., 2018). A few limitations that may add uncertainty remain to be taken into account with respect to the interpretation of WSIs. (1) The water stress generally is underestimated without the consideration of water quality while might be overestimated because of without water recycle. Severe water stress condition was rarely found in most southern areas of China when considering only water quantity, but it appeared due to poor water quality (Liu, Yang, et al., 2017). Degraded water quality can reduce the WA actually available for use and intensify water stress conditions in China (Jiang, 2009; Liu, Liu, et al., 2016). On the other hand, grey water may be used for nonpotable water use, which increases WA to some extent. However, water quality requirements often vary for different (potable or nonpotable) uses (Liu, Antonelli, et al., 2017; van Vliet et al., 2017), which will affect water recycling processes. Hence, the inclusion of them in water stress assessment remains a challenge. (2) Seasonal variations in hydrological regime (Hanasaki et al., 2013) and associated human intervention (e.g., reservoir regulation) can make the seasonal WA much different from the annual one. Previous studies (e.g., Veldkamp et al., 2016; Wada et al., 2011) suggested that it could be addressed by implementing a scheme of water stress assessment at a seasonal scale inside hydrological models. This would be critical to produce operational water stress assessment and understand the potential of human response toward mitigating water stress. (3) In this study, EFR is estimated with a straightforward approach but ignoring the different requirements from various hydrological regimes and river ecosystems (Pastor et al., 2014). More comprehensive EFR estimates will merit a water stress assessment toward regional sustainable development. (4) The absence of large-scale water transfers (e.g., the South-North Water Transfer Project) in GHMs will lead to underestimation (overestimation) of WA and thereby overestimated (underestimated) water stress in the target (source) basins. Inclusion of interbasin water transfer will help improve water stress assessment, especially over typical water-receiving areas such as urban areas. (5) The threshold used to define severe water stress can affect the water stress assessment (Hanasaki et al., 2018b), particularly the WSPOP estimates. The threshold of 0.4 for severe water stress conventionally takes into account EFR. Thus, severe water stress and the affected population defined by WSI > 0.4 might be overestimated. The additional analysis with the threshold of 0.6 shows that the WSPOP will be less than those using the threshold of 0.4 based on WSI_C, but the differences are small for the future period (see Table S6).

5. Conclusions

Water stress is assessed in China using multimodel simulations for the historical (1971–2010) and future (2021–2050) periods with specific attention to potential implications of the usage of different WSIs. In addition, our water stress simulations are compared to reported data for 10 major basins of China over the period 2001–2010 and show reasonable performance. The WSIs characterized by different WA show distinct spatial patterns in terms of both severe water stress and population under stress. Based on the WSI with consideration of consumption (WSI_C), we estimated that 368 million people (one third of the total population) per year was affected by severe water stress in the past. Without consideration of the upstream water resources, WSI based on runoff (WSI_R) estimates higher local water stress by more than 60% in terms of population compared to WSI_C. Without subtracting the consumptive parts of upstream water withdrawals, WSI based on natural streamflow (WSI_Q) estimates lower water-stressed population by up to 8% compared to WSI_C. The differences between the WSIs suggest that water use largely relies on the water resources from the river network where local water resources are scarce. In this study, WSI_C is relatively reasonable for future water stress assessment by considering both upstream water availability and consumptive water use. During the historical period, the northern basins have experienced severe water stress. In the next few decades, water stress would be more severe in many regions of China and would particularly expand in southern basins where so far very little water stress was found. The projections of WSI_C suggest that future severe water stress might appear in nearly 50% (with quartiles range from 40% to 56% across RCPs) of the total areas of China and more than 600 million (43% of the total; with quartiles range from 542 to 680 million across RCPs) people might be under severe stress. This study emphasizes the necessity of considering the upstream and downstream relations with respect to both water uses and water availability in water stress assessment and calls attention to the being intensified water stress in both northern and southern basins in China in the coming decades.

Acknowledgments
This research is supported by the National Natural Science Foundation of China (41877164, 41730645, 41790424, and 41625001) and the Strategic Priority Research Program of Chinese Academy of Sciences (XDA20060402). We thank the Inter-Sectoral Impact Model Intercomparison Project coordinating team for providing the multimodel simulations. All model data used in this study can be accessed by the public following the instructions on the Inter-Sectoral Impact Model Intercomparison Project website (www.isimip.org). The authors declare that they have no conflict of interest.

References

Alcamo, J., Henrichs, T., & Rösch, T. (2000). World water in 2025—Global modeling and scenario analysis for the World Commission on Water for the 21st century. Report A0002, Center for Environmental Systems Research, University of Kassel, pp 49.

Biemans, H., Haddeland, I., Kabat, P., Ludwig, F., Hutjes, R. W. A., Heinke, J., et al. (2011). Impact of reservoirs on river discharge and irrigation water supply during the 20th century. *Water Resources Research*, *47*, W03509. https://doi.org/10.1029/2009WR008929

Bondeau, A., Smith, P. C., Zaehle, S., Schaphoff, S., Lucht, W., Cramer, W., et al. (2007). Modelling the role of agriculture for the 20th century global terrestrial carbon balance. *Global Change Biology*, *13*(3), 679–706. https://doi.org/10.1111/j.1365-2486.2006.01305.x

Cai, X. (2008). Water stress, water transfer and social equity in Northern China—Implications for policy reforms. *Journal of Environmental Management*, *87*(1), 14–25. https://doi.org/10.1016/j.jenvman.2006.12.046.

Cai, J., Varis, O., & Yin, H. (2017). China's water resources vulnerability: A spatio-temporal analysis during 2003–2013. *Journal of Cleaner Production*, *142*, 2901–2910. https://doi.org/10.1016/j.jclepro.2016.10.180

Cheng, H., & Hu, Y. (2011). Economic transformation, technological innovation, and policy and institutional reforms hold keys to relieving China's water shortages. *Environmental Science & Technology*, *45*(2), 360–361. https://doi.org/10.1021/es1038744

Cheng, H., Hu, Y., & Zhao, J. (2009). Meeting China's Water Shortage Crisis: Current practices and challenges. *Environmental Science & Technology*, *43*(2), 240–244. https://doi.org/10.1021/es801934a

Flörke, M., Kynast, E., Bärlund, I., Eisner, S., Wimmer, F., & Alcamo, J. (2013). Domestic and industrial water uses of the past 60 years as a mirror of socio-economic development: A global simulation study. *Global Environmental Change*, *23*(1), 144–156. https://doi.org/10.1016/j.gloenvcha.2012.10.018

Frieler, K., Lange, S., Piontek, F., Reyer, C. P. O., Schewe, J., Warszawski, L., et al. (2017). Assessing the impacts of 1.5 °C global warming—Simulation protocol of the Inter-Sectoral Impact Model Intercomparison Project (ISIMIP2b). *Geoscientific Model Development*, *10*(12), 4321–4345. https://doi.org/10.5194/gmd-10-4321-2017

Gao, X., Schlosser, C. A., Fant, C., & Strzepek, K. (2018). The impact of climate change policy on the risk of water stress in southern and eastern Asia. *Environmental Research Letters*, *13*(6), 064039. https://doi.org/10.1088/1748-9326/aaca9e

Gosling, S., Müller Schmied, H., Betts, R., Chang, J., Ciais, P., Dankers, R., et al. (2017). ISIMIP2a Simulation Data from Water (global) Sector, GFZ Data Services. https://doi.org/10.5880/PIK.2017.010

Greve, P., Kahil, T., Mochizuki, J., Schinko, T., Satoh, Y., Burek, P., et al. (2018). Global assessment of water challenges under uncertainty in water scarcity projections. *Nature Sustainability*, *1*(9), 486–494. https://doi.org/10.1038/s41893-018-0134-9

Hanasaki, N., Fujimori, S., Yamamoto, T., Yoshikawa, S., Masaki, Y., Hijioka, Y., et al. (2013). A global water scarcity assessment under Shared Socio-economic Pathways-Part 2: Water availability and scarcity. *Hydrology and Earth System Sciences*, *17*(7), 2393–2413. https://doi.org/10.5194/hess-17-2393-2013

Hanasaki, N., Kanae, S., Oki, T., Masuda, K., Motoya, K., Shirakawa, N., et al. (2008a). An integrated model for the assessment of global water resources—Part 1: Model description and input meteorological forcing. *Hydrology and Earth System Sciences*, *12*(4), 1007–1025. https://doi.org/10.5194/hess-12-1007-2008

Hanasaki, N., Kanae, S., Oki, T., Masuda, K., Motoya, K., Shirakawa, N., et al. (2008b). An integrated model for the assessment of global water resources—Part 2: Applications and assessments. *Hydrology and Earth System Sciences*, *12*(4), 1027–1037. https://doi.org/10.5194/hess-12-1027-2008

Hanasaki, N., Yoshikawa, S., Kakinuma, K., & Kanae, S. (2016). A seawater desalination scheme for global hydrological models. *Hydrology and Earth System Sciences*, *20*(10), 4143–4157. https://doi.org/10.5194/hess-20-4143-2016

Hanasaki, N., Yoshikawa, S., Pokhrel, Y., & Kanae, S. (2018a). A global hydrological simulation to specify the sources of water used by humans. *Hydrology and Earth System Sciences*, *22*(1), 789–817. https://doi.org/10.5194/hess-22-789-2018

Hanasaki, N., Yoshikawa, S., Pokhrel, Y., & Kanae, S. (2018b). A quantitative investigation of the thresholds for two conventional water scarcity indicators using a state-of-the-art global hydrological model with human activities. *Water Resources Research*, *54*, 8279–8294. https://doi.org/10.1029/2018WR022931

Huang, Z., Hejazi, M., Li, X., Qiuhong, T., Vernon, C., Leng, G., et al. (2018). Reconstruction of global gridded monthly sectoral water withdrawals for 1971–2010 and analysis of their spatiotemporal patterns. *Hydrology and Earth System Sciences*, *22*(4), 2117–2133. https://doi.org/10.5194/hess-22-2117-2018

Jiang, Y. (2009). China's water scarcity. *Journal of Environmental Management*, *90*(11), 3185–3196. https://doi.org/10.1016/j.jenvman.2009.04.016

Jones, B., & O'Neill, B. C. (2016). Spatially explicit global population scenarios consistent with the Shared Socioeconomic Pathways. *Environmental Research Letters*, *11*(8), 084003. https://doi.org/10.1088/1748-9326/11/8/084003

Liu, C., Yu, J., & Eloise, K. (2001). Groundwater exploitation and its impact on the environment in the North China Plain. *Water International*, *26*(2), 265–272. https://doi.org/10.1080/02508060108686913

Liu, J., Liu, Q., & Yang, H. (2016). Assessing water scarcity by simultaneously considering environmental flow requirements, water quantity, and water quality. *Ecological Indicators*, *60*, 434–441. https://doi.org/10.1016/j.ecolind.2015.07.019

Liu, J., Yang, H., Gosling, S. N., Kummu, M., Flörke, M., Pfister, S., et al. (2017). Water scarcity assessments in the past, present, and future. *Earth's Future*, *5*, 545–559. https://doi.org/10.1002/2016EF000518

Liu, J., Zang, C., Tian, S., Liu, J., Yang, H., Jia, S., et al. (2013). Water conservancy projects in China: Achievements, challenges and way forward. *Global Environmental Change*, *23*(3), 633–643. https://doi.org/10.1016/j.gloenvcha.2013.02.002

Liu, W., Antonelli, M., Kummu, M., Zhao, X., Wu, P., Liu, J., et al. (2019). Savings and losses of global water resources in food-related virtual water trade. *Wiley Interdisciplinary Reviews Water*, *6*(1), e1320. https://doi.org/10.1002/wat2.1320

Liu, W., Antonelli, M., Liu, X., & Yang, H. (2017). Towards improvement of grey water footprint assessment: With an illustration for global maize cultivation. *Journal of Cleaner Production*, *147*, 1–9. https://doi.org/10.1016/j.jclepro.2017.01.072

Liu, X., Liu, W., Yang, H., Tang, Q., Flörke, M., Masaki, Y., et al. (2019). Multimodel assessments of human and climate impacts on mean annual streamflow in China. *Hydrology and Earth System Sciences*, *23*(3), 1245–1261. https://doi.org/10.5194/hess-23-1245-2019

Liu, X., Tang, Q., Cui, H., Mengfei, M., Gerten, D., Gosling, S., et al. (2017). Multimodel uncertainty changes in simulated river flows induced by human impact parameterizations. *Environmental Research Letters*, *12*(2), 025009. https://doi.org/10.1088/1748-9326/aa5a3a

Liu, X., Tang, Q., Voisin, N., & Cui, H. (2016). Projected impacts of climate change on hydropower potential in China. *Hydrology and Earth System Sciences*, *20*(8), 3343–3359. https://doi.org/10.5194/hess-20-3343-2016

Liu, X., Tang, Q., Zhang, X., & Leng, G. (2016). Modeling the role of vegetation in hydrological responses to climate change. In Q. Tang & T. Oki (Eds.), *Terrestrial Water Cycle and Climate Change: Natural and Human-Induced Impacts*, (pp. 193–208). Hoboken, New Jersey: John Wiley & Sons, Inc. https://doi.org/10.1002/9781118971772.ch10

Mekonnen, M. M., Hoekstra, A. Y. (2016). Four billion people facing severe water scarcity. *Science Advances*, *2*(2), 2117. https://doi.org/10.1126/sciadv.1500323

Müller Schmied, H., Adam, L., Eisner, S., Fink, G., Flörke, M., Kim, H., et al. (2016). Variations of global and continental water balance components as impacted by climate forcing uncertainty and human water use. *Hydrology and Earth System Sciences*, *20*(7), 2877–2898. https://doi.org/10.5194/hess-20-2877-2016

Müller Schmied, H., Eisner, S., Franz, D., Wattenbach, M., Portmann, F. T., Flörke, M., & Döll, P. (2014). Sensitivity of simulated global-scale freshwater fluxes and storages to input data, hydrological model structure, human water use and calibration. *Hydrology and Earth System Sciences*, *18*(9), 3511–3538. https://doi.org/10.5194/hess-18-3511-2014

Oki, T., & Kanae, S. (2006). Global hydrological cycles and world water resources. *Science*, *313*(5790), 1068–1072. https://doi.org/10.1126/science.1128845

Pastor, A. V., Ludwig, F., Biemans, H., Hoff, H., & Kabat, P. (2014). Accounting for environmental flow requirements in global water assessments. *Hydrology and Earth System Sciences*, *18*(12), 5041–5059. https://doi.org/10.5194/hess-18-5041-2014

Pokhrel, Y. N., Koirala, S., Yeh, P. J. F., Hanasaki, N., Longuevergne, L., Kanae, S., & Oki, T. (2015). Incorporation of groundwater pumping in a global Land Surface Model with the representation of human impacts. *Water Resources Research*, *51*, 78–96. https://doi.org/10.1002/2014WR015602

Rost, S., Gerten, D., Bondeau, A., Lucht, W., Rohwer, J., & Schaphoff, S. (2008). Agricultural green and blue water consumption and its influence on the global water system. *Water Resources Research*, *44*, W09405. https://doi.org/10.1029/2007WR006331

Schaphoff, S., Heyder, U., Ostberg, S., Gerten, D., Heinke, J., & Lucht, W. (2013). Contribution of permafrost soils to the global carbon budget. *Environmental Research Letters*, *8*(1), 014026. https://doi.org/10.1088/1748-9326/8/1/014026

Schewe, J., Heinke, J., Gerten, D., Haddeland, I., Arnell, N. W., Clark, D. B., et al. (2014). Multimodel assessment of water scarcity under climate change. *Proceedings of the National Academy of Sciences of the United States of America*, *111*(9), 3245–3250. https://doi.org/10.1073/pnas.1222460110

Sheffield, J., Goteti, G., & Wood, E. F. (2006). Development of a 50-Year High-Resolution Global Dataset of Meteorological Forcings for Land Surface Modeling. *Journal of Climate*, *19*(13), 3088–3111. https://doi.org/10.1175/jcli3790.1

Smakhtin, V., Revenga, C., & Döll, P. (2004). *Taking into account environmental water requirements in global-scale water resources assessments* (p. 32). Colombo, Sri Lanka: IWMI.

Takata, K., Emori, S., & Watanabe, T. (2003). Development of the minimal advanced treatments of surface interaction and runoff. *Global and Planetary Change*, *38*(1–2), 209–222. https://doi.org/10.1016/S0921-8181(03)00030-4

Tang, Q., Oki, T., Kanae, S., & Hu, H. (2007). The influence of precipitation variability and partial irrigation within grid cells on a hydrological simulation. *Journal of Hydrometeorology*, *8*(3), 499–512. https://doi.org/10.1175/jhm589.1

Tang, Q., Oki, T., Kanae, S., & Hu, H. (2008). Hydrological cycles change in the Yellow River basin during the last half of the twentieth century. *Journal of Climate*, *21*(8), 1790–1806. https://doi.org/10.1175/2007JCLI1854.1

Tang, Q., Zhang, X., & Tang, Y. (2013). Anthropogenic impacts on mass change in North China. *Geophysical Research Letters*, *40*, 3924–3928. https://doi.org/10.1002/grl.50790

van Vliet, M. T. H., Flörke, M., & Wada, Y. (2017). Quality matters for water scarcity. *Nature Geoscience*, *10*, 800. https://doi.org/10.1038/ngeo3047

Veldkamp, T. I. E., Wada, Y., Aerts, J. C. J. H., Döll, P., Gosling, S. N., Liu, J., et al. (2017). Water scarcity hotspots travel downstream due to human interventions in the 20th and 21st century. *Nature Communications*, *8*(1), 15697. https://doi.org/10.1038/ncomms15697

Veldkamp, T. I. E., Wada, Y., Aerts, J. C. J. H., & Ward, P. J. (2016). Towards a global water scarcity risk assessment framework: Incorporation of probability distributions and hydro-climatic variability. *Environmental Research Letters*, *11*(2), 024006. https://doi.org/10.1088/1748-9326/11/2/024006

Veldkamp, T. I. E., Wada, Y., de Moel, H., Kummu, M., Eisner, S., Aerts, J. C. J. H., & Ward, P. J. (2015). Changing mechanism of global water scarcity events: Impacts of socioeconomic changes and inter-annual hydro-climatic variability. *Global Environmental Change*, *32*, 18–29. https://doi.org/10.1016/j.gloenvcha.2015.02.011

Veldkamp, T. I. E., Zhao, F., Ward, P. J., de Moel, H., Aerts, J. C. J. H., Schmied, H. M., et al. (2018). Human impact parameterizations in global hydrological models improve estimates of monthly discharges and hydrological extremes: A multi-model validation study. *Environmental Research Letters*, *13*(5), 055008. https://doi.org/10.1088/1748-9326/aab96f

Vörösmarty, C. J., Douglas, E. M., Green, P. A., & Revenga, C. (2005). Geospatial indicators of emerging water stress: An application to Africa. *Ambio: A Journal of the Human Environment*, *34*(3), 230–236. https://doi.org/10.1579/0044-7447-34.3.230

Vörösmarty, C. J., Green, P., Salisbury, J., & Lammers, R. B. (2000). Global water resources: Vulnerability from climate change and population growth. *Science*, *289*(5477), 284–288. https://doi.org/10.1126/science.289.5477.284

Wada, Y., Flörke, M., Hanasaki, N., Eisner, S., Fischer, G., Tramberend, S., et al. (2016). Modeling global water use for the 21st century: The Water Futures and Solutions (WFaS) initiative and its approaches. *Geoscientific Model Development*, *9*(1), 175–222. https://doi.org/10.5194/gmd-9-175-2016

Wada, Y., van Beek, L. P. H., Viviroli, D., Dürr, H. H., Weingartner, R., & Bierkens, M. F. P. (2011). Global monthly water stress: 2. Water demand and severity of water stress. *Water Resources Research*, *47*, W07518. https://doi.org/10.1029/2010WR009792

Wada, Y., Wisser, D., & Bierkens, M. F. P. (2014). Global modeling of withdrawal, allocation and consumptive use of surface water and groundwater resources. *Earth System Dynamics*, *5*(1), 15–40. https://doi.org/10.5194/esd-5-15-2014

Wang, J., Li, Y., Huang, J., Yan, T., & Sun, T. (2017). Growing water scarcity, food security and government responses in China. *Global Food Security*, *14*, 9–17. https://doi.org/10.1016/j.gfs.2017.01.003

Wang, J., Zhong, L., & Long, Y. (2016). Baseline water stress: China, Technical Note, 16 pp, World Resources Institute, Beijing.

Yang, H., & Zehnder, A. (2001). China's regional water scarcity and implications for grain supply and trade. *Environment and Planning A: Economy and space*, *33*(1), 79–95. https://doi.org/10.1068/a3352

Weedon, G. P., Gomes, S., Viterbo, P., Shuttleworth, W. J., Blyth, E., Österle, H., et al. (2011). Creation of the WATCH Forcing Data and Its Use to Assess Global and Regional Reference Crop Evaporation over Land during the Twentieth Century, *Journal of Hydrometeorology*, *12*(5), 823–848. https://doi.org/10.1175/2011jhm1369.1

Weedon, G. P., Balsamo, G., Bellouin, N., Gomes, S., Best, M. J., & Viterbo, P. (2014). The WFDEI meteorological forcing data set: WATCH Forcing Data methodology applied to ERA-Interim reanalysis data, *Water Resources Research*, *50*, 7505–7514. https://doi.org/10.1002/2014WR015638

Zhao, X., Liu, J., Liu, Q., Tillotson, M. R., Guan, D., & Hubacek, K. (2015). Physical and virtual water transfers for regional water stress alleviation in China. *Proceedings of the National Academy of Sciences*, *112*(4), 1031–1035. https://doi.org/10.1073/pnas.1404130112